Euro. Jnl of Applied Mathematics: (2019), *vol.* 30, *pp.* 912–927
doi:10.1017/S0956792518000529

Theoretical and experimental study of a pendulum excited by random loads

L. DOSTAL and M.-A. PICK

Institute of Mechanics and Ocean Engineering, Hamburg University of Technology, 21073 Hamburg, Germany
email: dostal@tuhh.de, pick@tuhh.de

(*Received 16 January 2018; revised 25 July 2018; accepted 25 July 2018; first published online 18 September 2018*)

Results on the behaviour of a pendulum which is parametrically excited by large amplitude random loads at its pivot are presented, including a novel experimental case study. Thereby, it is dealt with a random excitation by a non-white Gaussian stochastic process with prescribed spectral density. Special focus is devoted to stochastic processes resulting from random sea wave elevation and the question whether random sea waves can lead to rotational motion of the parametrically excited pendulum. The motivation for such an experimental study is energy harvesting from ocean waves.

Key words: Parametric excitation, pendulum dynamics, stochastic averaging, experimental random excitation, energy harvesting

2010 Mathematics Subject Classification: 60H30, 60H10, 37N10

1 Introduction

The present analysis deals with the general dynamics of a randomly excited pendulum which is parametrically excited by large amplitude loads at its pivot. The parametric pendulum has a very rich dynamical behaviour [6] and has applications in various other problems, such as mechanical, electrical, microelectromechanical, optical and other systems, cf. [8,12]. Another fundamental problem involving random pendulum dynamics is energy harvesting from a source whose nature is random. Since wave energy has been recognised as one of the most promising resources of renewable energy due to the notably high power density [10], several new concepts of ocean wave energy converters were recently developed and studied [2,14]. One possible method of energy generation is to use ocean gravity waves to excite the pivot of a pendulum in order to induce and maintain rotational motion.

Due to its complicated nonlinear dynamics, there is still further research necessary if the source of excitation is random. In the case of harmonic excitation, approximate analytical solutions for oscillatory and rotational motion of a parametric pendulum were obtained in [15] by using the method of multiple scales. Because of the significant nonlinearity and the involved random excitation, researchers relied on numerical methods and Monte Carlo simulation in order to obtain new results for large amplitude oscillations of a randomly excited pendulum [1,11]. Recently, in [9], a pendulum which is acted on by a small additive white noise has been considered. In the same time, results on white and non-white parametric Gaussian noise excitation of a pendulum have been obtained in [5]. In the present study, we deal with pendulum motion in the case of excitation by a non-white Gaussian random process which results from a floating body in real sea states.

2 Tilted stochastic pendulum model

We are interested in the dynamical behaviour of a damped pendulum with lumped mass M at a distance l from the suspension point which is initially restricted to move vertically on a line with a vertical randomly time-varying displacement f. This line can be tilted together with the plane of oscillation of the pendulum by the angle $\theta = 90° - \beta$. The corresponding dynamical system can be represented by the following equation of motion:

$$Ml^2 \frac{\mathrm{d}^2\varphi}{\mathrm{d}\bar{t}^2} + b_1 \frac{\mathrm{d}\varphi}{\mathrm{d}\bar{t}} + b_2 \frac{\mathrm{d}\varphi}{\mathrm{d}\bar{t}} \left| \frac{\mathrm{d}\varphi}{\mathrm{d}\bar{t}} \right| + Mgl \sin\beta \sin\varphi = \frac{Ml}{\sin\beta} \frac{\mathrm{d}^2 f}{\mathrm{d}\bar{t}^2} \sin\varphi. \tag{2.1}$$

Here, φ is the pendulum angle, b_1 is a damping parameter, $\bar{t}$ is a standard (unscaled) time and $f(\bar{t})$ is the randomly time-varying vertical displacement of the suspension point. In order to account for nonlinearities in damping, a nonlinear damping term with the damping parameter b_2 is also included. For the random excitation of the suspension point, we introduce the noise intensity ν and a Gaussian stochastic process $\xi_{\bar{t}}$ with zero mean and spectral density $S_{\xi\xi}$ and set

$$\frac{\mathrm{d}^2 f}{\mathrm{d}\bar{t}^2} := \nu \xi_{\bar{t}}.$$

Due to the possibility of tilting the plane of oscillation and the direction of the pivot motion, the restoring force due to gravity is reduced to $Mgl \sin\beta$, which lowers the natural frequency of the pendulum. For example, if the pendulum is excited by a randomly varying force with a mean frequency of 1.6 rad/s, then the length l of the pendulum is around 15 m when it is tuned to meet the primary parametric resonance. With an inclination angle of $\beta = 9°$, the length reduces to about 2.4 m. Moreover, the displacement of the suspension point along the inclined plane is given by $f^*(\bar{t}) = f(\bar{t})/\sin\beta$ and therefore the amplitude of the excitation will be enhanced according to

$$\frac{\mathrm{d}^2}{\mathrm{d}\bar{t}^2} f^*(\bar{t}) = \frac{\mathrm{d}^2}{\mathrm{d}\bar{t}^2} \frac{f(\bar{t})}{\sin\beta},$$

if the angle β is lowered. Such a design has been proposed in [4,17] for a wave energy converter. Thereby, a floating body is mounted on an inclined ramp, such that the wave elevation induces a displacement $f^*(\bar{t})$ along the ramp, which is higher than the corresponding vertical displacement $f(\bar{t})$. The increased motion of the floating body is useful for the design of efficient wave energy converters.

3 Energy-based stochastic averaging of random pendulum dynamics

The stochastic averaging method has been well established as a powerful, approximate technique for prediction of the response statistics of nonlinear dynamical systems. This method is focused on the energy envelope process of the dynamics by which means the problem is simplified to a lower-dimensional problem. Using such a stochastic averaging procedure, a perturbation parameter $\varepsilon \ll 1$ is introduced in the pendulum model, equation (2.1). Then, the scaled system with $t = \varepsilon\bar{t}$ is given as

$$\begin{aligned} \frac{\mathrm{d}}{\mathrm{d}t} x &= y, \\ \frac{\mathrm{d}}{\mathrm{d}t} y &= -\alpha \sin x - \varepsilon(\gamma_1 y + \gamma_2 y|y|) + \sqrt{\varepsilon}\lambda\xi_t \sin x, \end{aligned} \tag{3.1}$$

https://doi.org/10.1017/S0956792518000529 Published online by Cambridge University Press

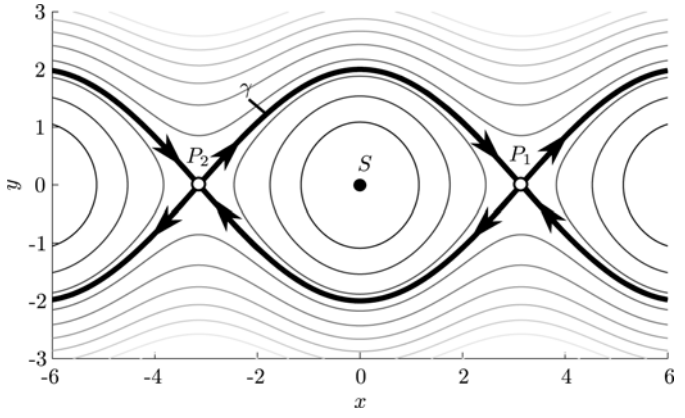

FIGURE 1. Contour lines of $H(x, y)$ for $\bar{\alpha} = 1$.

where we set $x = \varphi$ and $y = \dot{\varphi}$, using $\dot{\Psi} := \frac{\mathrm{d}}{\mathrm{d}t}\Psi$ as a shorthand for ε scaled time derivative, where Ψ is an arbitrary function of real numbers. Moreover, ξ_t is the corresponding time-scaled stochastic process and

$$\bar{\alpha} = \frac{g}{l}\sin\beta, \qquad \alpha = \frac{\bar{\alpha}}{\varepsilon^2}, \qquad \bar{\gamma}_1 = \frac{b_1}{Ml^2}, \qquad \gamma_1 = \frac{\bar{\gamma}_1}{\varepsilon^2}, \tag{3.2}$$

$$\bar{\gamma}_2 = \frac{b_2}{Ml^2}, \qquad \gamma_2 = \frac{\bar{\gamma}_2}{\varepsilon}, \qquad \bar{\lambda} = \frac{\nu}{l\sin\beta}, \qquad \lambda = \frac{\bar{\lambda}}{\varepsilon^{5/2}}. \tag{3.3}$$

We are interested in the total energy of the pendulum dynamics, which is given by the Hamilton function

$$H(x, y) := \frac{y^2}{2} + \alpha(1 - \cos x) = \frac{y^2}{2} + 2\alpha\sin^2\left(\frac{x}{2}\right). \tag{3.4}$$

The contour lines of the Hamilton function, $H(x, y)$ are shown in Figure 1. The fixed points of equation in equation (3.1) without dissipation and random perturbation (i.e. $\varepsilon = 0$) are

$$P_i = ((2i-1)\pi, 0)\,; \;\; S_i = (2i\pi, 0); \;\; i \in \mathbb{Z}. \tag{3.5}$$

Furthermore, the change in the total energy is the time derivative of the Hamilton function

$$\frac{\mathrm{d}}{\mathrm{d}t}H = -\varepsilon\left(\gamma_1 y^2 + \gamma_2 y^3\right) + \sqrt{\varepsilon}\,\lambda\xi_t y\sin x. \tag{3.6}$$

From the Hamiltonian function, we introduce the following relationship:

$$Q(x, H) := y^2 = 2H + 2\alpha(\cos x - 1) = 2H - 4\alpha\sin^2\left(\frac{x}{2}\right). \tag{3.7}$$

Then, combining the first equation of (3.1) and equation (3.5), the following system is obtained:

$$\begin{aligned} \frac{\mathrm{d}}{\mathrm{d}t}x &= \sqrt{Q(x, H)}, \\ \frac{\mathrm{d}}{\mathrm{d}t}H &= -\varepsilon\left(\gamma_1 + \gamma_2\sqrt{Q(x, H)}\right)Q(x, H) + \sqrt{\varepsilon}\,\lambda\xi_t\sqrt{Q(x, H)}\sin x, \end{aligned} \tag{3.8}$$

in which the variable y was eliminated by using the function $Q(x, H)$. The scaling parameter ε, in equation (3.1), helps to indicate the relative order of magnitude of the damping term

https://doi.org/10.1017/S0956792518000529 Published online by Cambridge University Press

and the external excitation term. An important property of the reformulated system in equation (3.7) is that the energy level H changes slowly compared to the oscillations of the variable x. This enables the application of the stochastic averaging method to this system, since the fast oscillatory dynamics can be averaged over the pendulum period.

Let H_c be the energy level corresponding to the separatrix γ between libration and rotation of the pendulum, as indicated in Figure 1. This energy level is given by $H_c = 2\alpha$. For the undisturbed libration motion of the pendulum, the period $T(H)$ at the energy level H $(0 \le H \le H_c)$ of one oscillation of the fast variable x in the absence of noise and damping (i.e. $\varepsilon = 0$) is given as [5]:

$$T(H) = \int_0^{T(H)} \mathrm{d}\tau = \frac{2}{\sqrt{\alpha}} \int_{-b(H)}^{b(H)} \frac{\mathrm{d}x}{\sqrt{k^2 - \sin^2\left(\frac{x}{2}\right)}} = \frac{4K(k)}{\sqrt{\alpha}}, \tag{3.9}$$

where K is the complete elliptic integral of the first kind, as described in [3], with elliptic modulus

$$k = \sqrt{\frac{H}{2\alpha}}. \tag{3.10}$$

The limits of integration $\pm b(H)$ in equation (3.8) are the points where $y = \sqrt{Q(x,H)} = 0$ and the periodic orbit intersects the x-axis, i.e. $b(H)$ is the maximum value of x for each energy level H and is given by

$$b = 2\arcsin(k). \tag{3.11}$$

We can now use stochastic averaging of the pendulum energy in the case of libration of the pendulum for the energy domain $H \in [0; 2\alpha)$, following [5]. Let therefore ξ_t in (3.1) be an absolutely regular zero-mean stationary stochastic process with sufficient mixing properties and autocorrelation $R_{\xi_t\xi_t}$. Let further H be the solution of system (3.7). Then, for fixed $0 \le H < 2\alpha$, the integrals

$$\begin{aligned} m(H) = {} & \frac{8\lambda^2 k^2}{\sqrt{\alpha}\, T(H)} \int_{-\infty}^{0} R_{\xi_t\xi_t}(s) \int_{-K(k)}^{K(k)} \mathrm{sn}\sqrt{1 - k^2\mathrm{sn}^2}\, \mathrm{sn}_{t+s} \sqrt{1 - k^2\mathrm{sn}_{t+s}^2}\, \frac{\mathrm{cn}_{t+s}}{\mathrm{cn}}\, \mathrm{d}u\, \mathrm{d}s \\ & + \frac{1}{T(H)} \int_0^{T(H)} Q(x(t), H) G(x(t), H) \mathrm{d}t, \end{aligned} \tag{3.12}$$

$$\sigma^2(H) = \frac{64\lambda^2 k^4 \sqrt{\alpha}}{T(H)} \int_{-\infty}^{\infty} R_{\xi_t\xi_t}(s) \int_0^{K(k)} \mathrm{sn}\sqrt{1 - k^2\mathrm{sn}^2}\, \mathrm{sn}_{t+s} \sqrt{1 - k^2\mathrm{sn}_{t+s}^2}\, \mathrm{cn}\mathrm{cn}_{t+s}\, \mathrm{d}u\, \mathrm{d}s \tag{3.13}$$

exist, and the process H converges, as $\varepsilon \to 0$, weakly on the time interval of order $\mathcal{O}(1/\varepsilon)$ to a diffusion Markov process H satisfying the Itô stochastic differential equation

$$\mathrm{d}H = m(H)\mathrm{d}t + \sigma(H)\mathrm{d}W_t. \tag{3.14}$$

Thereby, $\mathrm{d}W_t$ is a standard Wiener process, $m(H)$ is the drift, $\sigma(H)$ is the diffusion of equation (3.13) for the one-dimensional energy process H and

$$G(x, H) = -\left(\gamma_1 + \gamma_2\sqrt{Q(x, H)}\right). \tag{3.15}$$

https://doi.org/10.1017/S0956792518000529 Published online by Cambridge University Press

In equations (3.11) and (3.12), $\mathrm{sn}(\cdot, k)$ and $\mathrm{cn}(\cdot, k)$ are the Jacobian elliptic functions and the abbreviations $u := \sqrt{\alpha}t$, $\mathrm{sn} := \mathrm{sn}(u, k)$, $\mathrm{sn}_{t+s} := \mathrm{sn}(u + \sqrt{\alpha}s, k)$, $\mathrm{cn} := \mathrm{cn}(u, k)$ and $\mathrm{cn}_{t+s} := \mathrm{cn}(u + \sqrt{\alpha}s, k)$ are used.

4 First-passage probability

With the stochastic averaging results from Section 3, we have obtained a one-dimensional Itô stochastic differential equation for the pendulum energy H in the cases of libration. Using results on one-dimensional diffusion processes, we can state analytical formulas for the first-passage probabilities of the pendulum energy H.

Following [7], the differential generator $\mathcal{L}$ for a function $p(H)$ of the averaged process H defined by the Itô equation (3.13) is given by

$$\mathcal{L}p(H) = m(H)\frac{\partial}{\partial H}p(H) + \frac{1}{2}\sigma^2(H)\frac{\partial^2}{\partial H^2}p(H) \tag{4.1}$$

and the associated adjoint operator is

$$\mathcal{L}^*p(H) = -\frac{\partial}{\partial H}\left(m(H)p(H)\right) + \frac{1}{2}\frac{\partial^2}{\partial H^2}\left(\sigma^2(H)p(H)\right). \tag{4.2}$$

We introduce the scale measure

$$S(x) = \int^x s(y)\mathrm{d}y, \tag{4.3}$$

where

$$s(y) = \exp\left(-2\int^y \frac{m(\theta)}{\sigma^2(\theta)}\mathrm{d}\theta\right) \tag{4.4}$$

is the scale density. After defining the speed density

$$\mu(y) = 1/(\sigma^2(y)s(y)) \tag{4.5}$$

and the speed measure M by

$$\mathrm{d}M(y) = \mu(y)\mathrm{d}y, \tag{4.6}$$

we can transform the operator $\mathcal{L}$ to

$$\mathcal{L}p(H) = \frac{1}{2}\frac{\partial}{\partial M}\left(\frac{\partial p(H)}{\partial S}\right), \tag{4.7}$$

such that the drift is identically zero. We are interested in the first-passage probability of energy levels of the randomly excited parametric pendulum, in order to obtain the probability of reaching rotational pendulum motion starting from an initial energy level H_0. The necessary energy for rotational motion of the pendulum has to be greater than $H_c = 2\alpha$, which is the energy level at the heteroclinic orbit γ. Therefore, we consider the energy interval $[H_a; H_b]$, where $0 < H_a < H_b \leq H_c$. Following [7], the probability to reach the energy H_b before the energy H_a, starting at $H_0 \in [H_a; H_b]$ is the solution of the differential equation

$$\mathcal{L}u(H_0) = 0, \tag{4.8}$$

https://doi.org/10.1017/S0956792518000529 Published online by Cambridge University Press

with boundary conditions $u(H_a) = 0$ and $u(H_b) = 1$. The solution follows directly from two successive integrations of the corresponding transformed operator from equation (4.7) and is given by

$$u(H_0) = \frac{S[H_a, H_0]}{S[H_a, H_b]}, \tag{4.9}$$

where we have used the abbreviation

$$S[a, b] := \int_a^b s(y)\,\mathrm{d}y, \quad a, b \in \mathbb{R}. \tag{4.10}$$

With this result, we are able to calculate the first-passage probability to reach the energy H_c, where the pendulum starts to rotate, before reaching a very small energy level of small pendulum motion.

5 Pendulum wave energy converter

A possible physical application of our results is harvesting energy from ocean waves using a pendulum wave energy converter design. Therefore, we are also interested in a case study with realistic random excitation due to ocean waves. We assume that the pendulum energy converter is mounted on a floating body whose degrees of freedom are limited to heave and whose mass is much greater than the pendulum mass. With these assumptions, the influence of the pendulum motion on the heave motion is negligible. Moreover, we assume linear dynamics of the floating body. The parametric excitation due to ocean waves is modelled by a Gaussian stochastic process with a given spectral density. Various spectral densities were defined to describe different sea states.

Common sea spectral densities are the Pierson–Moskowitz spectrum for deep water waves and the JONSWAP spectrum for shallow water waves. We use the following two-parameter version of the JONSWAP spectrum with significant wave height H_s and modal frequency ω_m:

$$S_{\mathrm{jon}}(\omega) = 0.2059\, H_s^2\, \frac{\omega_m^4}{\omega^5} \exp\left\{-1.25\left(\frac{\omega_m}{\omega}\right)^4\right\} \gamma^{\exp\left\{-0.5(\omega-\omega_m)^2/(\sigma\omega_m)^2\right\}}, \tag{5.1}$$

where $\sigma = 0.07$ is set for $\omega < \omega_m$ and $\sigma = 0.09$ for $\omega > \omega_m$. The peak shape parameter γ is chosen as 3.3. The spectral density of the heave displacement of the floating body due to a JONSWAP sea state is given by

$$S_f(\omega) = |\mathrm{RAO}_f(\omega)|^2 S(\omega), \tag{5.2}$$

where

$$\mathrm{RAO}_f(\omega) = \frac{\hat{f}(\omega)}{-\omega^2(M + A_h(\omega)) + i\omega B_h(\omega) + C_h} \tag{5.3}$$

is the response amplitude operator (RAO) of the heave displacement of the floating body with the hydrodynamic excitation force complex amplitude per wave height $\hat{f}(\omega)$, mass M, added mass A_h, hydrodynamic damping B_h and restoring coefficient C_h. The hydrodynamic parameters $\hat{f}(\omega)$, $A_h(\omega)$, $B_h(\omega)$ and C_h can, for example, be determined by strip theory.

https://doi.org/10.1017/S0956792518000529 Published online by Cambridge University Press

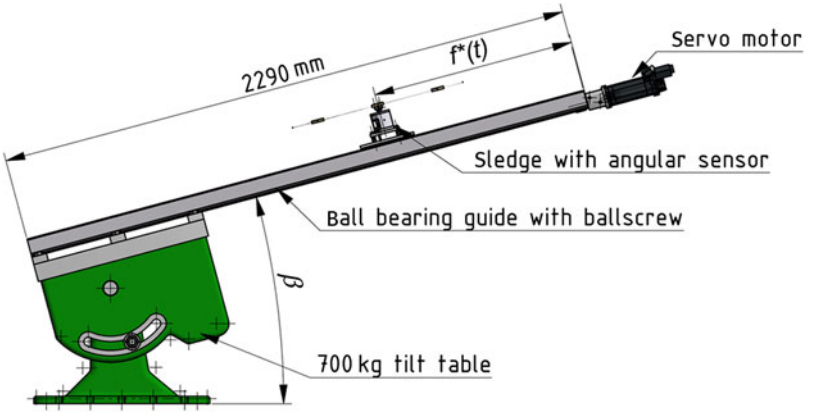

FIGURE 2. Sketch of the experimental setup of a pendulum energy converter, side view.

The heave acceleration RAO is easily obtained from $\mathrm{RAO}_f(\omega)$ by

$$\mathrm{RAO}_{\ddot{f}}(\omega) = \omega^2 \mathrm{RAO}_f(\omega). \tag{5.4}$$

The spectral density of the heave acceleration of the floating body due to a JONSWAP sea state is then given by

$$S_{\ddot{f}}(\omega) = |\mathrm{RAO}_{\ddot{f}}(\omega)|^2 S(\omega). \tag{5.5}$$

From a spectral density $S_{\xi\xi}(\omega)$ of a Gaussian process ξ, the corresponding autocorrelation function $R_{\xi\xi}$ is obtained by Fourier transformation, such that $R_{\xi\xi}$ can be used for the determination of $m(H)$ and $\sigma(H)$ in equations (3.11) and (3.12).

6 Experimental setup for a pendulum energy converter

The models and results from Sections 3 and 4 are evaluated by experiments. In preliminary studies [2,17], experimental setups with harmonic excitation using a motor driving a crank shaft were conducted. In our case, random excitations due to motions of a floating body in real sea states must be applied to the pendulum's pivot. Ocean wave-induced motions are low in frequency and require high amplitudes of the motion in order to achieve a certain level of acceleration. For this reason, the pivot is mounted onto a sled that is guided by a set of linear ball bearings, as sketched in Figure 2. The sled is driven by a ball screw with a thread of 10 mm per revolution. The ball screw itself is driven by a Siemens 1FT7034 high dynamic servomotor with a maximum rotational speed of 6000 rpm, so a maximum sled speed of 1000 mm/s can be achieved. The maximum travelling distance of the sled is 2000 mm. The motor is powered by a Siemens Sinamics S120 drive and controlled by a Siemens Simotion D435, so the difficult requirements on dynamics and accuracy of the desired motion are fulfilled. In order to realise any pivot motion from horizontal to vertical, the linear guides are mounted on a massive tilt table from a former boring and milling machine. This very stiff table's mass is about 700 kg and the tilt angle is adjusted very precisely by crank handle turning a worm gear. With these industrial components a rigid, simple and very flexible setup for experiments with one translational motion was created.

https://doi.org/10.1017/S0956792518000529 Published online by Cambridge University Press

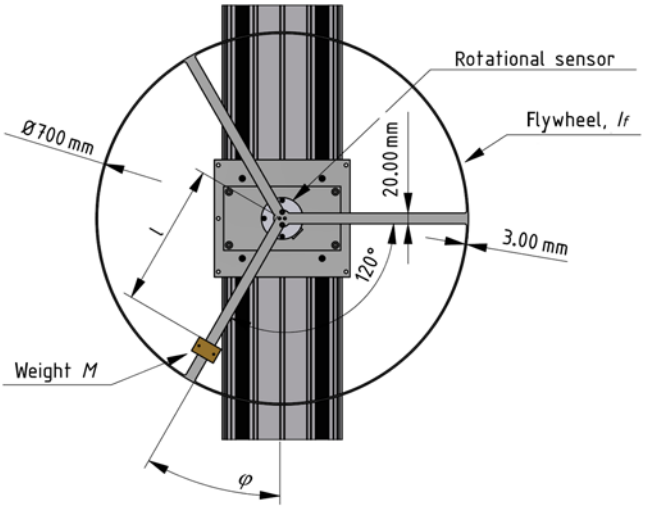

FIGURE 3. Sketch of the pendulum and the flywheel component mounted on the sled.

One major goal for the pendulum's design is a low eigenfrequency which is easily tunable in a wide range towards zero. This requirement is met using a balanced three-arm pendulum which is cut by laser from a 3-mm stainless steel sheet, as shown in Figure 3. For safety reasons and in order to increase the pendulum's stiffness and moment of inertia, the ends of the pendulum arms are connected by a 3-mm circular flywheel. In this configuration, there is no certain position of equilibrium and the lowest possible eigenfrequency is achieved. Adding weight to the arms, the pendulum gets unbalanced and nearly every eigenfrequency below a maximum one can be achieved by adjusting the weights at each arm individually [5,16]. The experiments described here were done with one weight as shown in Figure 3. The distance from the weight's centre of gravity to the pivot is l. The pendulum's pivot is realised by shaft mounted between a set of smooth running roller bearings, just oiled, not greased. The pendulum is mounted to the shaft's upper end with two bolts. Between the bearings, a contactless magnetic induction encoder (Zettlex Incoder) is placed in order to measure the rotation angle φ of the pendulum with a resolution of 16 bit per revolution. As the Zettlex Incoders are absolute encoders, no referencing at the beginning of an experiment is required. The encoder signals are digital according to the Synchronous Serial Interface standard. Data of the sled's kinematic are received from the Simotion controller by Profibus with a frequency of 50 Hz. With this frequency, the set point for the sled's velocity is sent to the controller. The time vector of position or velocity set points is precalculated for every experiment as we assume no influence of the pendulum's motion on the pivot's motion. The total view of the experimental rig is shown in Figure 4 and a picture of the pendulum and the flywheel component of the experimental rig is given in Figure 5.

The processing of the measurements and the Profibus communication is done by a National Instruments compact reconfigurable input-output real-time device programmed in Labview. With the chosen setup the best results for a smooth motion were achieved by sending velocity instead of position setpoints. Due to mechanical restrictions in acceleration and jerk, negligibly small drift of the pivot's position can be observed which is shown in Figure 6. In order to better maintain rotational motion of the pendulum, a flywheel is added whose moment of inertia is denoted

https://doi.org/10.1017/S0956792518000529 Published online by Cambridge University Press

FIGURE 4. Experimental rig of the pendulum energy converter.

as I_f. This changes the total moment of inertia of the rotating part to $(Ml^2 + I_f)$. In addition to the damping coefficients c and d, we consider a generator with a nonlinear function for the torque T_g due to energy generation, given by $T_g = c_g\dot{\varphi} + d_g\dot{\varphi}\,|\dot{\varphi}|$. The resulting equation of motion for the angle φ of the pendulum can be written as

$$(Ml^2 + I_f)\frac{\mathrm{d}^2\varphi}{\mathrm{d}\bar{t}^2} + (c + c_g)\frac{\mathrm{d}\varphi}{\mathrm{d}\bar{t}} + (d + d_g)\frac{\mathrm{d}\varphi}{\mathrm{d}\bar{t}}\left|\frac{\mathrm{d}\varphi}{\mathrm{d}\bar{t}}\right| + Ml\left(g\sin\beta + \frac{1}{\sin\beta}\frac{\mathrm{d}^2 f}{\mathrm{d}\bar{t}^2}\right)\sin(\varphi) = 0, \quad (6.1)$$

using again the vertical displacement $f(t)$ of the pendulum pivot and the pendulum mass M as in equation (2.1). With this, the scaling coefficients in equation (3.2) for the dynamics of the experimental rig have to be changed to

https://doi.org/10.1017/S0956792518000529 Published online by Cambridge University Press

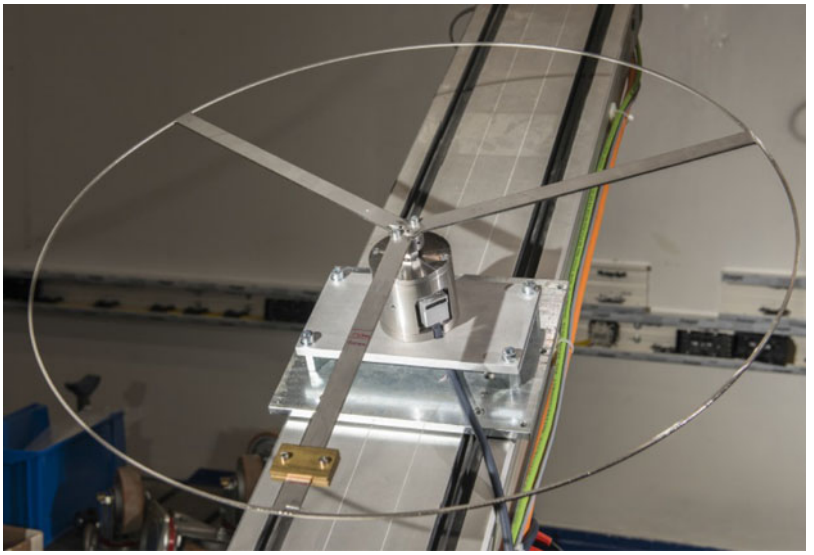

FIGURE 5. Pendulum and the flywheel component of the experimental rig.

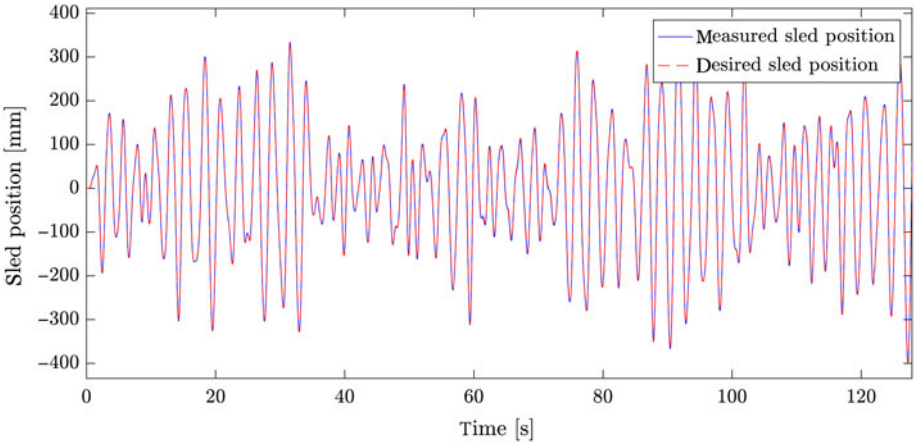

FIGURE 6. Comparison between the desired random trajectory of the sled and the measured sled position during experimental run.

$$\bar{\alpha} = \frac{Mgl}{Ml^2 + I_f} \sin\beta, \qquad \alpha = \frac{\bar{\alpha}}{\varepsilon^2}, \qquad \bar{\gamma}_1 = \frac{b_1}{Ml^2 + I_f}, \qquad \gamma_1 = \frac{\bar{\gamma}_1}{\varepsilon^2},$$
$$\bar{\gamma}_2 = \frac{b_2}{Ml^2 + I_f}, \qquad \gamma_2 = \frac{\bar{\gamma}_2}{\varepsilon}, \qquad \bar{\lambda} = \frac{\nu Ml}{(Ml^2 + I_f)\sin\beta}, \qquad \lambda = \frac{\bar{\lambda}}{\varepsilon^{5/2}}, \tag{6.2}$$

in order to arrive at the scaled equation (3.1). The harvestable electrical power P_{el} of such a pendulum energy converter is the product of the generator torque T_g, the angular velocity $\dot{\varphi}$ and the energy conversion efficiency η of the generator, such that

$$P_{\mathrm{el}} = \eta\, T_g\, \dot{\varphi}. \tag{6.3}$$

https://doi.org/10.1017/S0956792518000529 Published online by Cambridge University Press

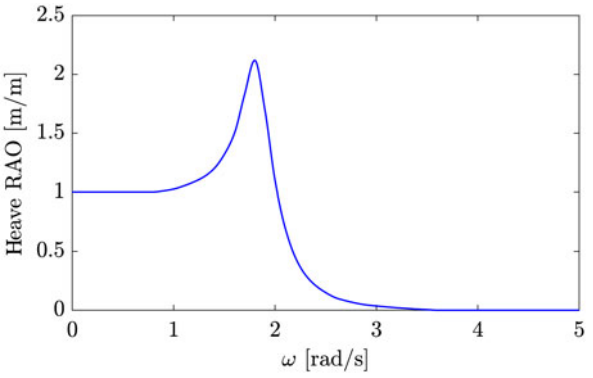

FIGURE 7. Vertical heave displacement RAO $|\mathrm{RAO}_f|$ of a vertical cylinder.

7 Theoretical and experimental results

With the theory from Sections 3 and 4, we calculate the first-passage probability of the pendulum to reach the energy H_c, where the pendulum starts to rotate, before reaching a very small energy level of small pendulum motion.

In order to produce the highest amount of electrical energy, the pendulum has to reach rotational motion. Therefore, we need to set up the pendulum, such that the probability to reach rotational motion is as high as possible for the given random excitation. We consider JONSWAP sea states with arbitrary significant wave heights H_s and different modal frequencies ω_m. As the floating body, we use a vertical cylinder which is described in [13]. A wave elevation induces forces and moments on a floating body. Assuming linear dynamics, the heave displacement spectral density $S_f(\omega)$ of the floating cylinder is determined using equation (5.2). Thereby, the heave displacement RAO of the vertical cylinder is used, as shown in Figure 7. An example wave elevation for a JONSWAP sea state with $H_s = 0.19\,\mathrm{m}$ and $\omega_m = 1.4$ rad/s is shown in Figure 8(a). A typical heave displacement time series of the floating cylinder in such a JONSWAP sea state is shown in Figure 8(b). Note, that this time series was generated from the corresponding spectrum $S_f(\omega)$ and not from the wave elevation as shown in Figure 8(a). As can be seen in Figure 8, typical wave excitations lead to dynamics of the floating body, which significantly deviate from a harmonic excitation. Thereby, the floating body response can be seen as a filter of the wave excitation input.

Using equation (4.9), we have calculated the first-passage probability of the pendulum for variable initial energy levels H_0 and the set of fixed parameters

$$\bar{\alpha} = 1,\ \bar{\gamma}_1 = 0.01,\ \bar{\gamma}_2 = 0.$$

Results for the variation of the first-passage probability with respect to initial pendulum energy H_0 and different modal frequencies ω_m are shown in Figure 9, for a fixed $\bar{\lambda} = 0.1$ and for a fixed $\bar{\lambda} = 0.16$ in Figure 10. Thereby, the random excitation process ξ is normalised, such that its spectrum is a JONSWAP spectrum with $H_s = 1$. Then the desired significant wave height H_s is adjusted by setting the noise intensity to $\nu = H_s$ [m]. In addition, we have calculated the first-passage probability for a fixed low initial energy of $H_0 = 0.2$, variable $\bar{\lambda}$, and different modal frequencies ω_m, as shown in Figure 11. It can be seen from these figures that a region with a high probability of reaching rotational motion of the pendulum exists for the chosen

https://doi.org/10.1017/S0956792518000529 Published online by Cambridge University Press

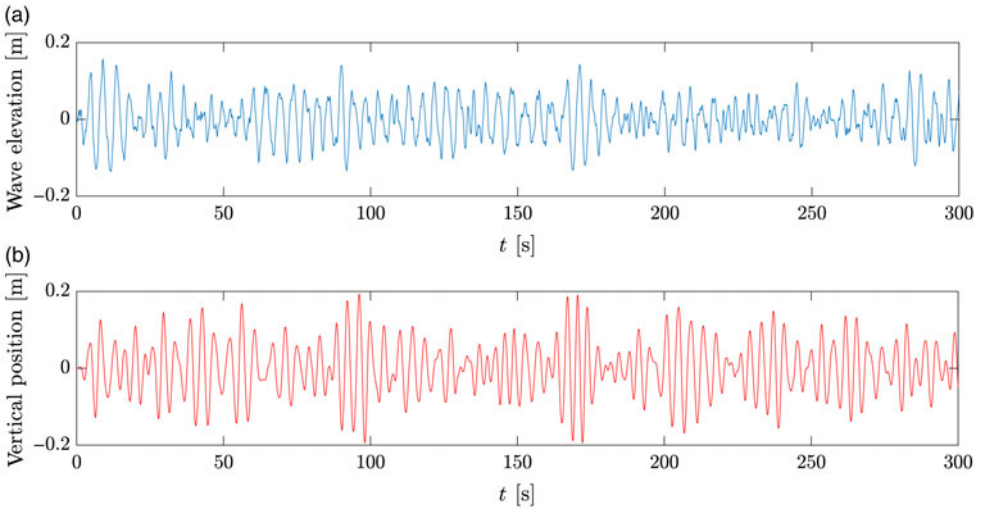

FIGURE 8. For a JONSWAP sea state with $H_s = 0.19$ m and $\omega_m = 1.4$ rad/s, a typical wave elevation is shown in (a) and a typical time series of the vertical position of a floating cylinder with RAO according to Figure 7 is shown in (b).

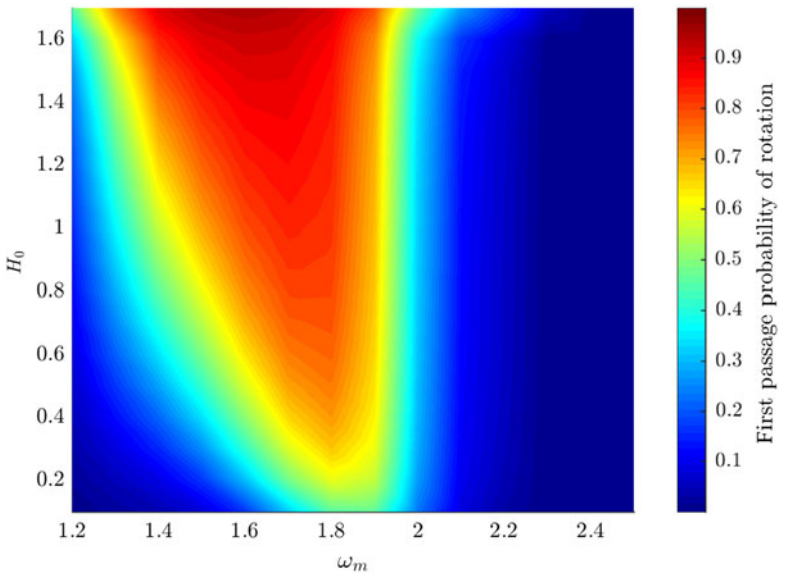

FIGURE 9. Variation of first-passage probability with respect to initial pendulum energy H_0 and different modal frequencies ω_m, for a JONSWAP sea state with $\bar{\lambda} = 0.1$, $\bar{\gamma}_1 = 0.01$, $\bar{\gamma}_2 = 0$ and $\mathrm{RAO}_{\bar{f}}$.

parameter set. We also observe regions with almost zero probability for reaching rotational motion. Based on these results, we have chosen specific parameters for the initial energy level H_0, the modal frequency ω_m and significant wave height H_s of the JONSWAP sea state, as well as the following parameters for the experimental setup:

$$M = 0.1\,\mathrm{kg}, \qquad l = 0.15\,\mathrm{m}, \qquad I_f = 0.036\,\mathrm{kg\,m^2}, \qquad \beta = 15^\circ. \tag{7.1}$$

https://doi.org/10.1017/S0956792518000529 Published online by Cambridge University Press

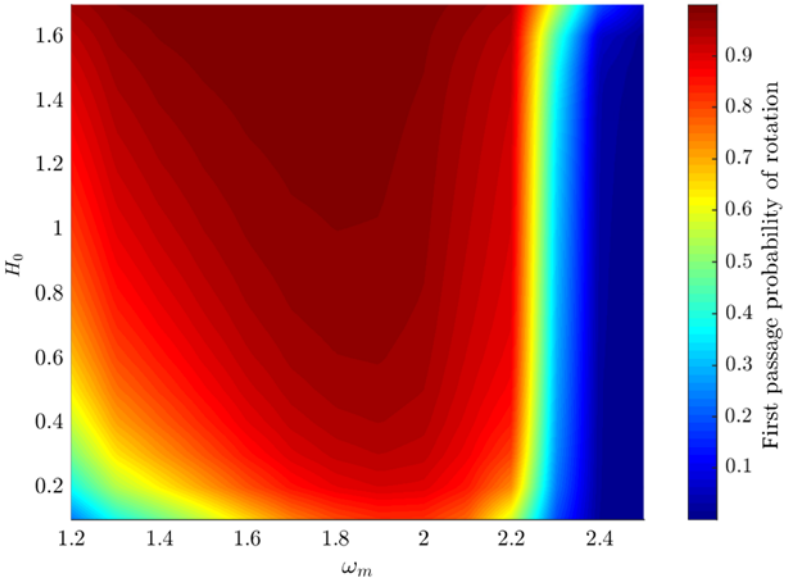

FIGURE 10. Variation of first-passage probability with respect to initial pendulum energy H_0 and different modal frequencies ω_m, for a JONSWAP sea state with $\bar{\lambda} = 0.16$, $\bar{\gamma}_1 = 0.01$, $\bar{\gamma}_2 = 0$ and $\mathrm{RAO}_{\bar{f}}$.

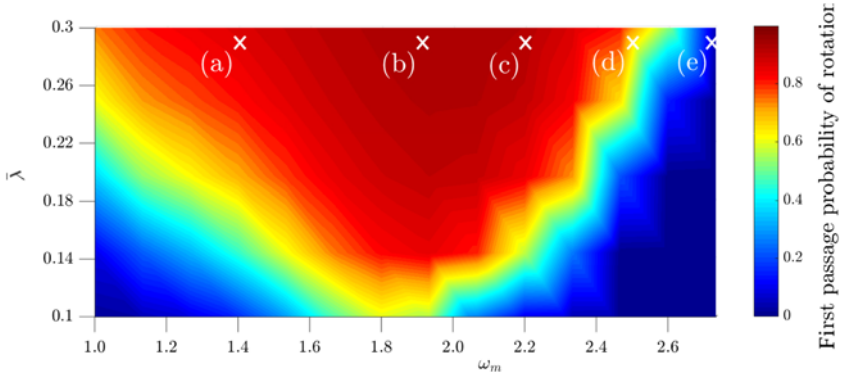

FIGURE 11. First-passage probability map for low initial energy $H_0 = 0.2$ and a JONSWAP sea state with variable $\bar{\lambda}$, different modal frequencies ω_m, $\bar{\gamma}_1 = 0.01$, $\bar{\gamma}_2 = 0$ and $\mathrm{RAO}_{\bar{f}}$. The parameter combinations of $\bar{\lambda}$ and ω_m, which were used for the experiments from Figure 12, are marked by a white cross.

Then we have generated the corresponding time series for the large amplitude random excitation. As can be seen in Figure 6, an influence of the pendulum dynamics on the sled position during experimental runs is not observed and the error between the measured sled position and the desired sled position is very small and insignificant.

As the outcome of the experiment, we have measured the random time series of pendulum angle φ in JONSWAP sea states with the modal frequencies $\omega_m = 1.4$, 1.9, 2.2, 2.5, 2.7, 3.0 rad/s and a significant wave height of 19 cm, which corresponds to $\bar{\lambda} = 0.29$ for the parameter set in equation (7.1). The first-passage probabilities for this choice of parameters are marked in Figure 11 by white crosses. The results are shown in Figure 12, where a sufficient percentage of rotational motion can be observed for the cases (a)–(d). As has been predicted by first-passage

https://doi.org/10.1017/S0956792518000529 Published online by Cambridge University Press

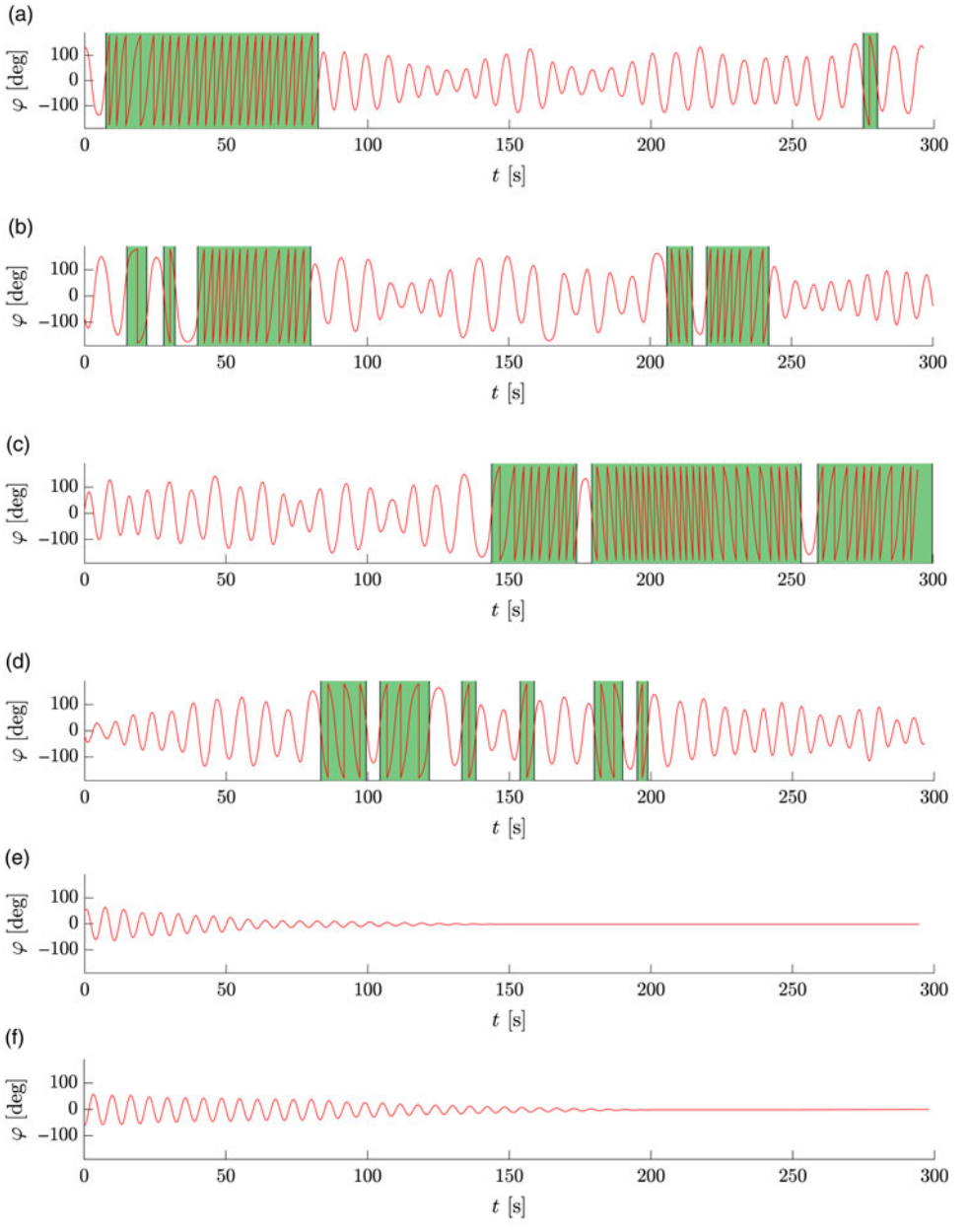

FIGURE 12. Measured pendulum angle for a sled trajectory due to a JONSWAP wave elevation with $H_s = 19$ cm and (a) $\omega_m = 1.4$ rad/s, (b) $\omega_m = 1.9$ rad/s, (c) $\omega_m = 2.2$ rad/s, (d) $\omega_m = 2.5$ rad/s, (e) $\omega_m = 2.7$ rad/s and (f) $\omega_m = 3.0$ rad/s. The green regions indicate rotation of the pendulum.

probability results in Figure 11, these results show that it is possible to generate a rotational motion of the pendulum due to large amplitude parametric excitation in the proposed experiment.

We have also obtained experimental results for an eigenfrequency $\bar{\alpha} = 1.3$ of the pendulum, which was obtained by setting the parameters of the experimental rig to

$$M = 0.1\,\text{kg}, \qquad l = 0.30\,\text{m}, \qquad I_f = 0.036\,\text{kg}\,\text{m}^2, \qquad \beta = 15^\circ.$$

https://doi.org/10.1017/S0956792518000529 Published online by Cambridge University Press

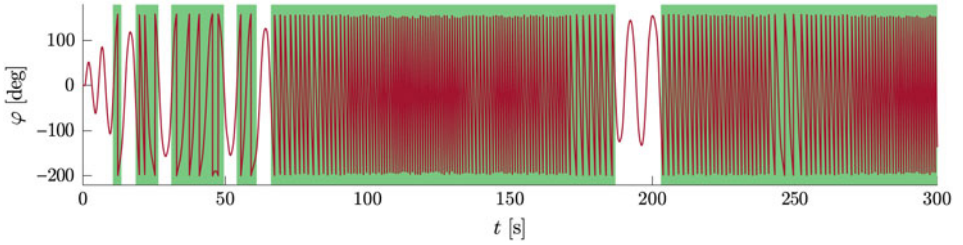

FIGURE 13. Measured pendulum angle for a sled position along the inclined rail due to a JONSWAP wave elevation with $H_s = 12.5$ cm and $\omega_m = 2.4$ [rad/s]. The green regions indicate rotation of the pendulum.

For this case, a time series of the pendulum angle is shown in Figure 13, resulting from a random motion of the pendulum pivot due to a JONSWAP wave elevation with significant wave height $H_s = 12.5$ cm and modal frequency $\omega_m = 2.4$ rad/s. The green regions indicate rotation of the pendulum which occurs with a percentage of 89.5. This percentage is large considering the small significant wave height of the wave elevation.

8 Conclusion

Specific results on the random dynamics of a pendulum are obtained, including random excitation due to ocean waves. It is also shown that rotational motion of a specific inclined pendulum setup is possible even for low-to-moderate random excitation, including excitation due to random ocean waves. Experimental results for the proposed pendulum setup which is excited by a large amplitude random excitation were not obtained before.

Conflict of interest

None.

References

[1] ALEVRAS, P. & YURCHENKO, D. (2014) Stochastic rotational response of a parametric. *Prob. Eng. Mech.* **37**, 124–131.

[2] ALEVRAS, P., BROWN, I. & YURCHENKO, D. (2015) Experimental investigation of a rotating parametric pendulum. *Nonlinear Dyn.* **81**(1–2), 201–213.

[3] BYRD, P. F. & FRIEDMAN, M. D. (1954) *Handbook of Elliptic Integrals for Engineers and Scientists*, B.G. Teubner, Berlin.

[4] DOSTAL, L. & PICK, M.-A (2017) Power generation of a pendulum energy converter excited by random loads. In: *Proceedings of the 9th European Nonlinear Oscillations Conference*, Congressline Ltd., Budapest, Hungary.

[5] DOSTAL, L., KORNER, K., KREUZER, E. & YURCHENKO, D. (2018) Pendulum energy converter excited by random loads. *ZAMM – J. Appl. Math. Mech.* **98**(3), 349–366. doi:10.1002/zamm.201700007.

[6] HORTON, B., WIERCIGROCH, M. & XU, X. (2008) Transient tumbling chaos and damping identification for parametric pendulum. *Philos. Trans. R. Soc. A* **366**(1866), 767–784.

[7] KARLIN, S. & TAYLOR, M. H. (1981) *A Second Course in Stochastic Processes*, Academic Press, New York.

[8] LANDAU, L. D. & LIFSHITZ, E. M. (2007) *Mechanics*, Elsevier, Oxford.

https://doi.org/10.1017/S0956792518000529 Published online by Cambridge University Press

[9] LINGALA, N., SRI NAMACHCHIVAYA, N., SAUER, P. W. & YEONG, H. C. (2017) Random perturbations of nonlinear oscillators: homogenization and large deviations. *Int. J. Non-Linear Mech.* **94**(Suppl. C), 235–250 (Special issue: A conspectus of nonlinear mechanics: a tribute to the oeuvres of Professors G. Rega and F. Vestroni).
[10] MCCORMICK, M. E. (2013) *Ocean Wave Energy Conversion*, Courier Corporation, New York.
[11] NAJDECKA, A., NARAYANAN, S. & WIERCIGROCH, M. (2015) Rotary motion of the parametric and planar pendulum under stochastic wave excitation. *Int. J. Non-Linear Mech.* **71**, 30–38.
[12] NAYFEH, A. H. & MOOK, D. T. (2008) *Nonlinear Oscillations*, John Wiley & Sons, New York.
[13] SHENG, W. & LEWIS, A. (2012) Assessment of wave energy extraction from seas: numerical validation. *J. Energy Resour. Tech.* **134**(4), 041701.
[14] VAZIRI, V., NAJDECKA, A. & WIERCIGROCH, M. (2014) Experimental control for initiating and maintaining rotation of parametric pendulum. *Eur. Phys. J. Spec. Top.* **223**(4), 795–812.
[15] XU, X. & WIERCIGROCH, M. Approximate analytical solutions for oscillatory and rotational motion of a parametric pendulum. *Nonlinear Dyn.* **47**(1–3), 311–320.
[16] YURCHENKO, D. & ALEVRAS, P. (2013) Dynamics of the n-pendulum and its application to a wave energy converter concept. *Int. J. Dyn. Control* **1**(4), 290–299.
[17] YURCHENKO, D. & ALEVRAS, P. (2018) Parametric pendulum based wave energy converter. *Mech. Syst. Signal Process.* **99**, 504–515.

https://doi.org/10.1017/S0956792518000529 Published online by Cambridge University Press